Propagation Problems in Satellite Navigation

A. Hornbostel

DLR, Institute of Communications and Navigation

***Abstract*— Satellite navigation is based on measuring the signal delay between transmission at the satellite and reception by the user receiver. Therefore, the modeling and correction of the additional delay due to the propagation through the atmosphere and mitigation of signal disturbances in the user environment play an important role for the accuracy of the derived position solution. The paper provides an overview about the mechanisms of the main propagation phenomena which are relevant for satellite navigation, their magnitude, temporal and regional variation and standard methods to correct and mitigate them.**

***Index Terms*—Error Correction, Ionosphere, Multipath, Satellite Navigation Systems, Troposphere**

I. Introduction

The positioning with satellite navigation systems like GPS or Galileo is based on time of arrival measurements of the signals transmitted from the satellite at the receiver. The measured signal delays are converted to pseudo ranges by multiplication with the speed of light. The prefix 'pseudo' signifies the fact that these ranges do not correspond to the real geometrical distances to the satellites, because the receiver clock is not synchronized to the satellite system time and the measured delays include additional contributions by system and propagation errors which must be corrected for. For synchronization of the receiver clock to the system time measurement data from at least four satellites must be available. Then the receiver clock bias can be solved for as a fourth unknown together with the three unknown co-ordinates of the position *x, y, z* by triangulation. While system errors can normally not be corrected in real time, propagation errors can be reduced by models or advanced signal processing, where the remaining error depends on the type of measurements e.g. single frequency or dual frequency measurements, signal characteristics e.g. carrier frequency and bandwidth, and the quality of the models used.

Satellite navigation signals are extremely weak when they arrive at the user antenna; the nominal GPS power received at ground is -157 dBW, which is below the noise level. Therefore, the signals are sensitive to shadowing by buildings or vegetation. Navigation signal are spread spectrum signals, which are recovered from noise by dispreading in the receiver, i.e. by correlation with a replica of the satellite code. By this correlation process also the time of arrival, i.e. the delay of the received satellite code is determined. If the direct signal is superposed with reflected signals from the user environment due to multipath propagation, the peak of the correlation function becomes less unique and the accuracy of the delay measurement is reduced.

Table I shows an error budget for the GPS standard positioning services with the L1 C/A code. Shown is the User Equivalent Range Error (UERE), which is the RMS range error that the user must expect in the average worldwide. Note, that these are the residual errors after applying corrections.

In the table the main error contributions besides orbit and satellite clock errors are by propagation effects in the atmosphere and multipath propagation in the user environment. For single frequency measurements in L-Band the ionosphere error is even the dominant contributor in the whole error budget. The UERE budget demonstrates the importance of propagation modeling and improvement of correction models for high accuracy navigation, in particular when orbit and clock errors will be reduced by the technological progress in future systems like Galileo and modernized GPS. Therefore, the objective of this paper is to provide an overview about the characteristics of the main propagation effects and common correction and mitigation methods.

TABLE I
GPS L1 C/A Error Budget (UERE) [1]

Component	Error
Ephemeris	2.1 m
Satellite clock	2.1 m
Ionosphere	4.0 m
Multipath	1.4 m
Troposphere	0.7 m
Receiver noise	0.5 m
Total (RMS)	5.3 m

II. Propagation Path through the Atmosphere

Fig. 1 shows the propagation path of the signals through the different layers of the atmosphere. Within these layers the signal path and the propagation speed is influenced by the variation and gradient of the refractive index. Starting from the top, the signals first reach the ionosphere, where due the existence of free electrons the refractive index is smaller than

A. Hornbostel is with the Institute of Communications and Navigation at the German Aerospace Center (DLR e.V.), Oberpfaffenhofen, D-82230 Weßling, P.O. Box 1116, Germany (phone: +49 8153 282318, fax:+49 8153 282328, email: achim.hornbostel@dlr.de).

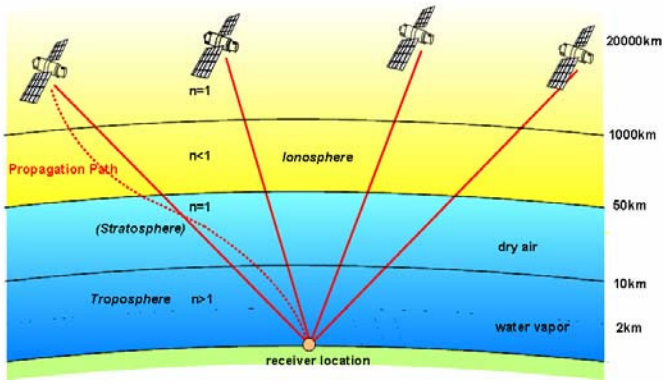

Fig. 1. Structure of the atmosphere and influence on propagation path.

one. The effect is that the group velocity of the signals is lowered compared to the vacuum but the phase velocity is enhanced. The concentration of free electrons increases with lower altitudes, where the highest concentration is around 300 km above the earth surface, and then decreases again. The corresponding gradient of the refractive index causes a curvature of the propagation path as shown in the figure as dotted line.

Between 50 and 100 km above ground the free electrons disappear and the signals start to propagate through the neutral atmosphere which is composed of different atmospheric gases. With lower altitudes the air pressure and density of the atmospheric gases increase and the refractive index grows accordingly to values larger than 1. The gradient of the refractive index again causes a curvature of the propagation path, which however is in the opposite direction as in the ionosphere. Here both the group velocity and the carrier velocity are slowed down compared to the vacuum speed of light.

The lower part of the neutral atmosphere, the troposphere extends from 0 to about 8 km at the poles, from 0 to about 13 km in mid latitudes and from 0 up to 18 km at the equator. It has the main contribution to the signal delay because it is the densest layer and contains most of the air mass and practically the total amount of water vapor of the atmosphere. Therefore, in the navigation community the delay in the neutral atmosphere is usually just called troposphere delay. The contribution to the signal delay by the water vapor, the so-called wet delay, makes only about 10% of the total troposphere (i.e. neutral atmosphere) delay. However, due to the high temporal and local variability of the water vapor, it is the most crucial component for modeling and error correction. The troposphere is also the region where the daily weather phenomena take place. In the lower troposphere additionally clouds, rain and fog exist. However, their influence on the amplitude and propagation velocity of the signals is negligible in L-band, where current and planned satellite navigation systems operate.

The sum of propagation delay and path curvature results in an excess path measured by the receiver compared to the true geometrical range. The excess path can be computed by integration of the refractive index along the curved path s through the atmosphere:

$$\Delta L = \int_S (n(s)-1)ds \ . \tag{1}$$

Often the excess path is just called delay in meters. If not corrected, the excess path is equivalent to an error of the same amount in the range measurements. For the normal navigation user, however, the profile of the refractive index along the path or even with height is not known and correction models are required, which do not require this information.

III. Ionosphere Error

A. Total Electron Content and Ionosphere Delay

The ionosphere is characterized by ions and free electrons which are created by UV and X-ray radiation of the sun. Therefore, the ionosphere state is coupled to the 11 year cycle of solar activity, to day and night time and to the season. The relevant layer which contains most of these particles extends between 80 and 1000 km above the earth surface. The key parameter for navigation is the Total Electron Content TEC, which is the integral of the total electron content in a column of 1m² from the observation point to the satellite:

$$TEC = \int_{path} N_e dl \quad [\text{el/m}^2\,] \,. \tag{2}$$

The ionospheric excess path is directly proportional to the TEC and inversely proportional to the square of the carrier frequency [2], [3], [4]:

$$\Delta L = \pm \frac{40.3}{f^2} \int_{path} N_e dl = \pm \frac{40.3}{f^2} TEC \,. \tag{3}$$

The plus sign applies for the group delay which is relevant for the code phase measurements of the navigation signals and the minus applies for the phase delay which is relevant for the carrier phase measurements. The opposite sign of code and carrier delay means that code and carrier diverge in the ionosphere, because the code is delayed but the carrier phase is advanced.

TABLE II
Ionosphere Excess Path

Frequency	TEC=10^{16} el/m²	TEC=10^{18} el/m²
100 MHz	40 m	4030 m
400 MHz	2.5 m	250m
1200 MHz	0.28 m	28 m
1600 MHz	0.16 m	16 m
5000 MHz	0.016m	1.6m

Table 2 shows typical values of the ionosphere excess path dependent on the carrier frequency for low and high TEC values. The vertical excess path lies normally between these values. The GPS, GLONASS and Galileo frequencies are between 1200 and 1600 MHz.

B. Temporal and Regional Behaviour

The TEC and correspondingly the ionosphere delay depend on the 11-year cycle of solar activity; they reache maximum values every 11 years. The last solar maximum was in the year 2000. The amplitude of the ionosphere delay depends also on the season, where highest values occur in winter (winter anomaly).

The ionosphere delay is highest in the so-called Crest region, which covers the latitudes between +/-20 degree around the geomagnetic equator, and in polar regions [4].

C. Dual Frequency Correction

If signals on two measurement frequencies are available the TEC value or directly the ionosphere error at each of these frequencies can be determined by measurement of their differential group delay $\delta(\Delta t) = \Delta t_2(f_2) - \Delta t_1(f_1)$. By division with the speed of light c from (3) follows:

$$\delta(\Delta t) = \frac{40.3}{c} TEC\left(\frac{1}{f_2^2} - \frac{1}{f_1^2}\right) = \Delta t_1 \frac{f_1^2 - f_2^2}{f_2^2}, \tag{4}$$

$$\Delta t_1 = \frac{f_2^2}{f_1^2 - f_2^2}\delta(\Delta t), \tag{5}$$

$$\Delta t_2 = \frac{f_1^2}{f_1^2 - f_2^2}\delta(\Delta t). \tag{6}$$

The dual frequency measurements are affected by all other errors on the measurement path. As long as they do not cancel out in the difference, these errors are multiplied with the frequency ratio $f_i^2/(f_1^2-f_2^2)$ with i=1,2. Therefore, the two measurement frequencies should not be too close to each other. For instance, for dual frequency corrections on GPS L_1=1.575GHz with help of the second frequency L_2=1.227 GHz the ratio is 1.54. The accuracy of the dual frequency correction is limited by the receiver noise and is in the order of 1 ns.

D. Single Frequency Correction Model

Single frequency users require a correction model which predicts the ionosphere error without measurement data. The most common model is the Klobuchar model [5], [6]. It models the daily behaviour dependent on user location, year, day of year and hour of day t, with help of 8 coefficients which are transmitted in the GPS navigation message. The daily behaviour of the ionospheric group delay t_g is modelled by a half-cosine function, with maximum amplitude at 14:00 o'clock local time.

$$t_g = F \cdot \left(5 + A\cos[2\pi(t-14)/P]\right)\,[\text{ns}] \quad \text{for } (t\text{-}14)/P < 1/4 \tag{7}$$

At night time with $(t\text{-}14)/P > 1/4$ the ionosphere group delay is set to constant value of 5 ns. The amplitude A and period P of the cosine function depend on user location and date. F is the mapping function which maps the vertical delay to the slant path delay. P is the period of day. The amplitude and period P are both approximated by polynomials of third degree with the ionospheric subpoint as input variable. This is the geomagnetic latitude, where the slant path from the user to the satellite crosses the ionospheric layer with highest electron density at 350 km height. The coefficients of the polynomials are transmitted to the user in the GPS navigation message. The mapping function F is [6]:

$$F = 1 + 2\left(\frac{96 - E}{90}\right)^3, \tag{8}$$

where E is the elevation angle of the satellite in degrees from the user point of view.

The advantage of the Klobuchar model is that it is easy to implement and requires only a few input parameters. However, the drawback is that its accuracy is only about 50%. Therefore, the ionosphere error is the dominant contribution in the error budget for single frequency GPS users.

E. EGNOS and WAAS

One reason for the introduction of the American Wide Area Augmentation System (WAAS) and the European Global Navigation Overlay System (EGNOS) was the reduction of the ionosphere error for single frequency GPS users. These systems derive the ionospheric error in a grid from dual frequency measurements in a regional ground station network and transmit differential corrections and integrity data via geostationary satellites. Because the information is distributed via satellites, these augmentation systems are also called Satellite Based Augmentation Systems (SBAS) in contrast to Local Area Augmentation Systems (LAAS), where local corrections and integrity data are transmitted from ground stations (GBAS), e.g. in the vicinity of an airport.

F. Doppler Shift

Temporal gradients of the TEC cause an additional Doppler shift measured by the receiver:

$$\Delta f = \frac{dn}{dt} = \frac{40.3}{cf}\frac{dTEC}{dt}. \tag{9}$$

An upper limit of the TEC rate for stationary users is 10^{15} el/m² per second. The corresponding frequency change is 0.085 Hz and the velocity error (range rate error) 1.6 cm/s [4].

IV. TROPOSPHERE ERROR

A. Refractivity and Delay

Introducing the refractivity $N = 10^6 (n\text{-}1)$, where n is the refractive index, (1) can be rewritten as:

$$\Delta L = 10^{-6} \int_{S_{tropo}} N(s)ds \,, \tag{10}$$

In this section only the curved path S_{tropo} through the neutral atmosphere is considered and ΔL is the troposphere excess path.

The refractive index of the neutral atmosphere is [7]:

$$N = 77.6\frac{P_d}{T} + 64.8\frac{P_w}{T} + 3.776\cdot 10^5 \frac{P_w}{T^2} = N_d + N_w \,, \tag{11}$$

where P_d is the partial pressure of dry air in hPa,, P_w is the partial pressure of water vapor in hPa and T is the temperature in K. N can be separated in a dry part N_d depending on P_d and T and in a wet part depending on P_w and T. Assuming that the air behaves as an ideal gas, alternatively, N can be split in a hydrostatic component depending only on the total air pressure P=P_d + P_w and a wet component depending again on water vapor and temperature [8],[9]. Note, that in both cases the wet components are slightly different, because the hydrostatic component contains also a small fraction depending on water vapor.

Common correction models do not apply (10) directly, but calculate the tropospheric delay from measured or predicted values of the refractive index at ground. For instance, the well-known Hopfield model [10] computes the dry and wet components of the zenith delay L^Z from the surface values of the dry and wet refractivity components N_{ds} and N_{ws} and two different scale heights H_d and H_w and then maps both components to the slant path delay by multiplication with two mapping functions $m_d(E)$ and $m_w(E)$, where E is the elevation angle of the path to the satellite, compare Fig. 2.:

$$\Delta L^Z = \Delta L_d^Z + \Delta L_w^Z = \frac{10^{-6}}{5}(N_{ds}H_d + N_{ws}H_w) \,, \tag{12}$$

$$\Delta L(E) = \Delta L_d^Z \cdot m_d(E) + \Delta L_w^Z \cdot m_w(E) \,. \tag{13}$$

The wet scale height is set to a constant value around 13000 m and the dry scale height is computed from the temperature in K at ground:

$$h_d = 148.98(T - 4.11) \,. \tag{14}$$

Most other models work in a similar manner. A special class of models, the so-called blind models, does not require estimated or measured meteorological input data and computes the surface refractivity and the corresponding zenith delay depending on user location and day of the year by regression formulas derived from global statistics of surface refractivity of pressure, water vapor and temperature.

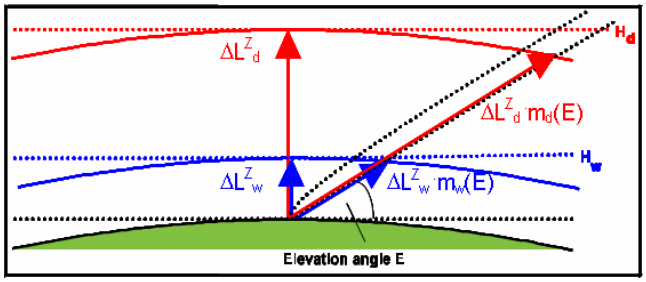

Fig. 2 Calculation of zenith delay and slant path delay.

B. Regional and Temporal Behavior of Tropospheric Delay

Typical values of the total zenith tropospheric delay (ZTD) for a ground-based user at heights near mean sea level are about 2.3 - 2.5 m. Although the wet delay contributes normally only with 5% - 15% to the total delay, the high temporal and spatial variability of the water vapor in the troposphere makes the wet delay to the most crucial component if accuracies in the decimeter or centimeter range are required.

Fig. 3 and Fig. 4 show the variation of the total zenith delay for Milan and Hong-Kong versus the day of year averaged over 10 years derived from measured daily radiosonde profiles of temperature, pressure and water vapor content with (10) and (11). For details of the radiosonde data bank and data processing see [11].

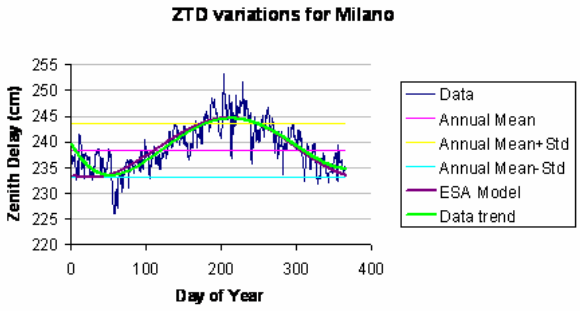

Fig. 3 10 years average of total tropospheric zenith path delay vs. day of year for Milan (Italy).

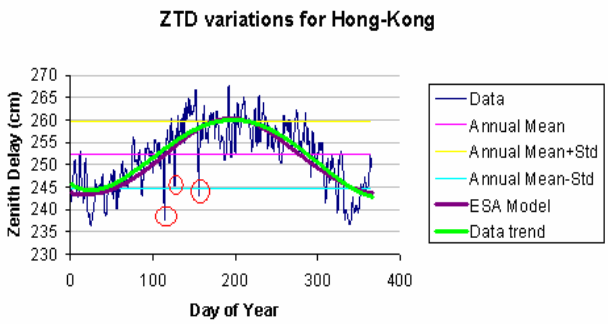

Fig. 4 10 years average of total tropospheric zenith path delay vs. day of year for Hong-Kong. The red circles mark some exceptional spikes, which even appear in the 10-year average.

The curves show that there is a seasonal variation with maximum in summer and minimum in winter, but there is also daily variation of about 5-10 cm around the mean trend. The seasonal dependence and the short time variations are both mainly due to the variation of the water vapor content. Due to the high atmospheric water vapor content in tropical areas the zenith delay in these areas is highest. The figures show also the data trend by curve fitting with a polynomial and a comparison with a model presented by ESA in [12].

C. *Comparison of Correction Models*

Fig. 6 shows a comparison of the 1-sigma residual error of the zenith path delay calculated with different tropospheric correction models [10],[13]-[22]. The 1-sigma error represents the error which is not exceeded for 68% of time; in most cases it is close to the RMS-error [23]. Reference data were again the 10 years radiosonde measurements from 11 globally distributed stations. The accuracy of the reference zenith path delay is in the order of 1 cm [11]. The figure provides results for non-blind models, where the measured surface values of temperature, air pressure and water vapor pressure have been used as input, and blind models which do not require such input data, see section IV.A. In the global mean the error for most models is about 3.5-4 cm, but there are locations were it exceeds 5 cm. It should be remembered here, that the non-blind models provide this accuracy only if accurately measured meteorological input data are available; this is often is not the case. Therefore, it is interesting to note, that the

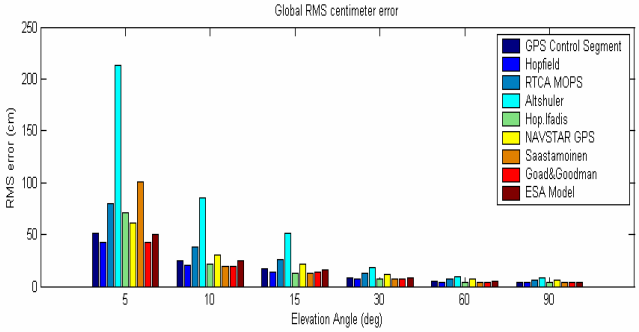

Fig. 5 RMS error vs. elevation angle for different correction models, average of 11 globally distributed stations and 10 years of radiosonde data [23].

ESA blind model [21], [22] performs nearly as well as the non-blind models and also the RTCA-MOPS Model [20] is not significantly worse for most locations. For the NAVSTAR-GPS Model [17] and the Altshuler Model [18], [19] it can be observed that they fail for high altitudes like Mexico City which is approx. 2200 m above mean sea level.

The error of the zenith path delay may appear not significant, but it is multiplied with the mapping function for other elevation angles and the mapping functions itself can introduce an additional error for low elevation angles [24], [23]. Fig. 5 provides the RMS-error of the different models in dependence of the elevation angle. With exception of one model, the different mapping function show more ore less the same performance for elevation angles > 10° and the resulting error can be kept below 30-40 cm. However, for lower

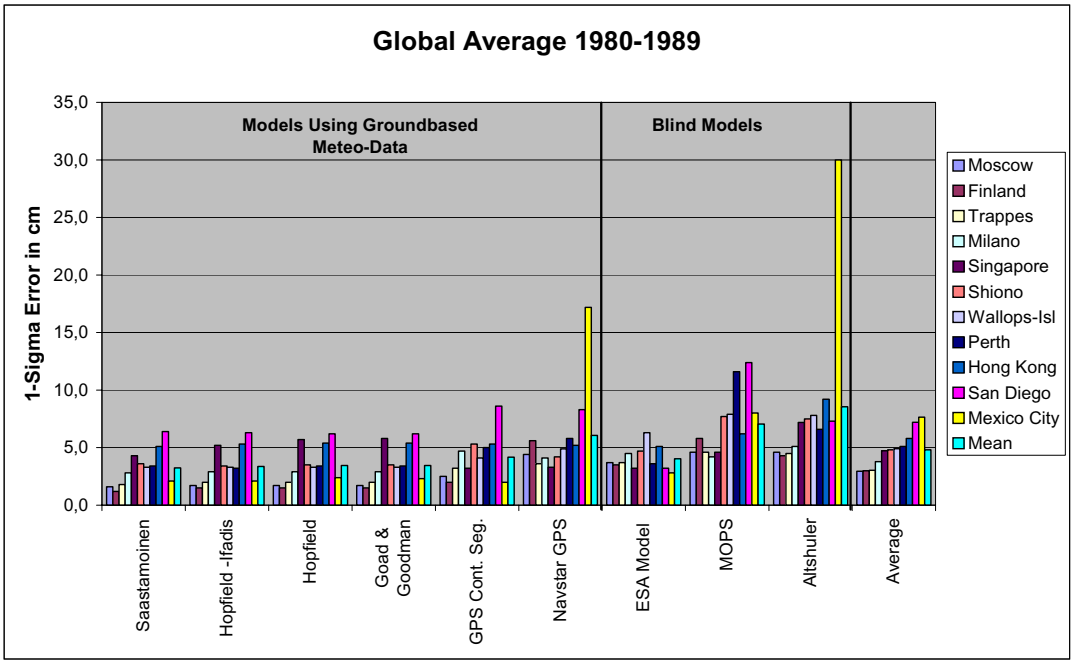

Fig. 6 Comparison of 1-sigma (68% confidence level) model performance for 11 globally distributed stations [23].

elevation angles, there are significant differences.

D. Local Events

In the previous sections the longtime average error of the correction models has been considered. However, for real time applications the instantaneous error and the rate of change of the error count. In particular the blind models can not follow the actual weather behavior at the user location due to their pure statistical nature. Fig. 7 shows an example of a local event recorded in Oberpfaffenhofen, Germany. In this event rapid changes of temperature, humidity and air pressure occurred during a thunderstorm front which passed the measurement site, e. g. the temperature dropped down from 32 degrees to 14 degrees and the air pressure fell by 9 hPa during the hours before the event and reached its original value after the event had passed. Accordingly, the tropospheric zenith delay predicted by the models using recorded data from ground based meteorological sensors changed by about 10 cm with in some hours and raised about 5 cm within less than an hour. When comparing with reference zenith delays from the IGS network which were computed by post-processing of GPS measurements, which were recorded also in Oberpfaffenhofen close to the site of the meteorological sensors, it is obviously that there are significant differences even to the non-blind real time models. The IGS results are considered to be accurate in the order of 0.5 cm [25]. It seems that the change of delay is over-predicted by the non-blind models. In [11], [23] a number of such events in Oberpfaffenhofen have been analyzed and it was found that maximum model errors of 8-10 cm occurred both for blind and non-blind models and that also during event periods the non-blind models perform only slightly better than the blind models.

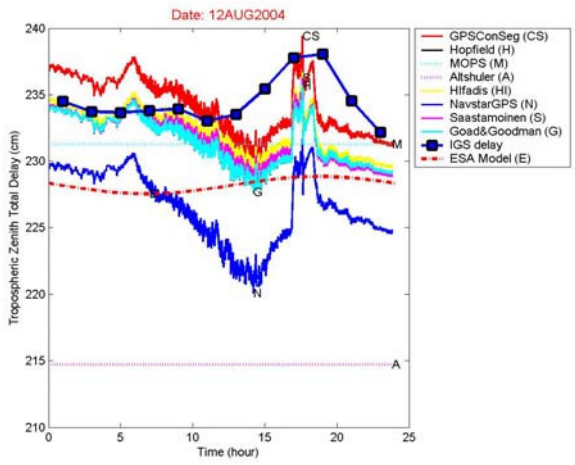

Fig. 7 Comparison of zenith delay computed with different tropospheric models during a thunderstorm passage in Oberpfaffenhofen, Germany.

V. Scintillations

Scintillations are fast fluctuations of signal amplitude and phase due to atmospheric turbulences, which occur irregularly and are difficult to predict in advance. The main part of the frequency spectrum of these fluctuations lies between 1 Hz to 10 Hz. Scintillations occur both due to ionopheric sources, i.e. fast TEC variations, or tropospheric sources, here mainly due to water vapor fluctuations or clouds. Tropospheric scintillations are only significant for low elevation angles, where mainly the amplitude scintillations are of concern. For instance they can reach 2.5 dB for 0.01% of time in tropical areas for an elevation angle of 5° according to the model in [26]. The RMS ranging error due to tropospheric phase fluctuations is below 1 cm for elevation angles above 5° [27].

Ionospheric scintillations are more critical, where both amplitude and phase scintillation can reach significant values. In tropical areas amplitude scintillation can cause signal fades of more than 20 dB so that the signals are completely lost by the receiver. In polar and aural regions amplitude scintillations due to geomagnetic storms can reach amplitudes around 10 dB, but here scintillation events can last several hours or even days. Phase scintillations occur mainly in tropical areas, but can also appear in mid latitudes during major magnetic storms. They lead to cycle slips, which are critical for carrier phase navigation, but can also lead to random phase fluctuations which exceed the narrow bandwidth of the receiver PLL (typically around 1 Hz) so that the receiver loses phase lock [4]. Similar as the regular ionosphere delay error, ionospheric scintillations depend on the solar activity and are strongest in tropical and polar regions.

VI. Shadowing

Signal attenuations due to atmospheric gases, cloud and rain are negligible in L-Band. However navigation signals can easily be attenuated by vegetation and walls or completely be shadowed by buildings and other obstacles. The specific attenuation for woodland at 1.6 GHz (ca. GPS L1) is about 0.3 dB/m [28]. Some values for attenuation by walls are given in Table III. Attenuation by walls is a particular problem for indoor navigation. However, methods have been developed to enhance the sensitivity of receivers by advanced signal processing. Indoor navigation can also be assisted by other means, e.g. by sending of a priori information via mobile communication links to the navigation receivers or by aiding with other sensors.

TABLE III
Attenuation by Walls [29], [30]

Type of building	Attenuation
Dwelling houses:	5 – 15 dB
Historical buildings:	25 - 35 dB
Office buildings:	30 dB
Underground garages:	> 30 dB

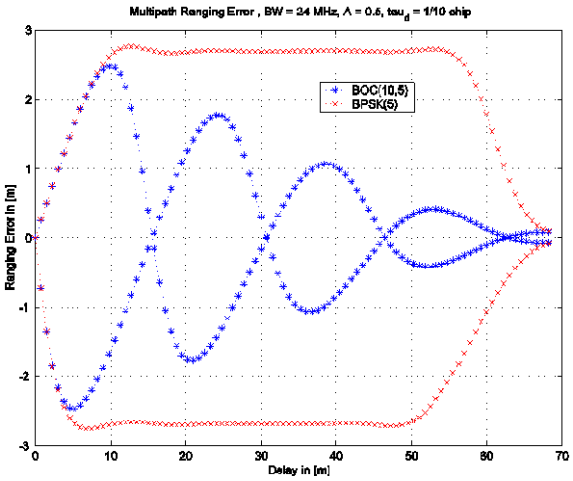

Fig. 8 Multipath error envelope. The picture shows the envelope of the resulting ranging error derived from receiver simulations for one multipath signal with half amplitude of the line-of-sight signal vs. the delay of the echo. The receiver bandwidth is 24 MHz and the correlator spacing is 0.1 code chip. Red: BPSK signal with 5MHz chip rate, blue: BOC-signal with 5*1.023 MHz chip rate and 10*1.023 MHz subcarrier modulation [31].

VII. Multipath

Signals which are reflected by the ground, buildings or other obstacles and superpose with the direct signal at the user antenna disturb the correlation function and reduce the ranging accuracy. The error depends on the amplitude, phase and the delay of the echo relative to the line-of-sight signal. Fig. 8 shows the error envelopes for a BPSK and a binary offset carrier signal (BOC), when one multipath signal with half amplitude of the line-of-sight signal is superposed with the line-of-sight signal.

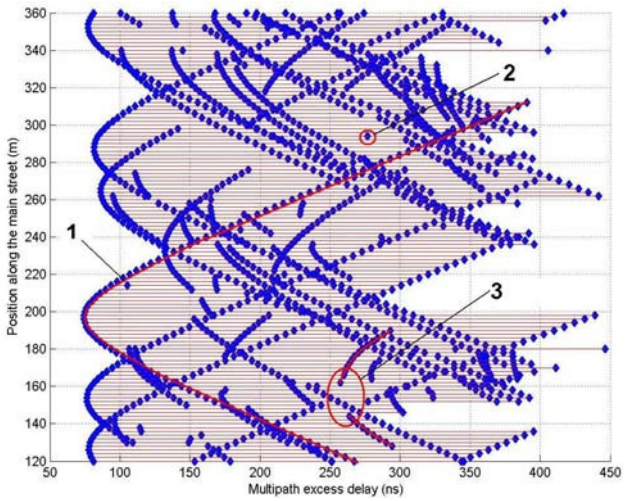

Fig. 9. Simulated multipath echoes for a car driving through an urban environment. The y-axis shows the position of the car in the main street of Fig. 10, the x-axis the delay of the echoes relative to the line-of-sight signal. The echoes are presented by blue symbols. The red marks highlight echoes with long (1), very short (2) and short (3) lifetime [32].

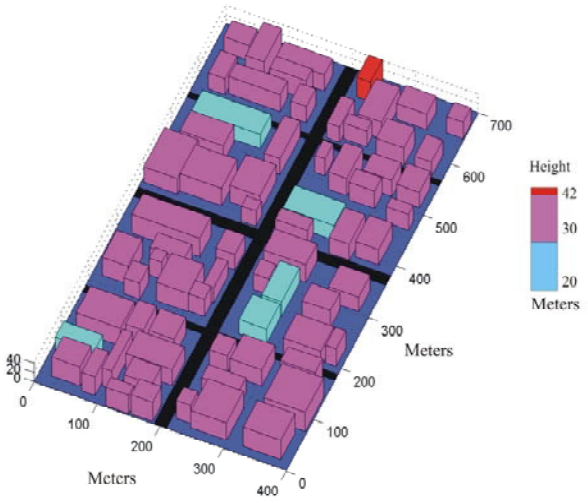

Fig. 10 Synthetic urban environment used in Fig. 8. Height and distribution of buildings are simulated based on probability density functions. The car drives along the main street [32].

The envelopes represent the maximum error which occurs when the multipath signal is in phase or in opposite phase (180°) with the line of sight signal. For all other phases the error lies between the envelopes. The figure illustrates also, that BOC signals are more robust against multipath propagation than BPSK signals.

In real environments normally several multipath signal are present simultaneously. Fig. 9 shows a simulation of the development of multipath signals for a car that drives through the synthetic urban environment illustrated in Fig. 10. Some echoes exist relatively long, whereas others have only a short or very short lifetime.

VIII. Conclusion

In satellite navigation the modeling and correction of the additional delay due to the propagation through the atmosphere and errors due to further propagation phenomena play an important role for the accuracy of the derived position solution. The largest additional signal delay occurs within the ionosphere. Because the ionosphere delay depends on frequency, it can be precisely determined and nearly completed eliminated by dual frequency measurements. However, for single frequency receivers, like most commercially available mass market GPS-receivers, the ionosphere delay must be corrected by modeling, and a significant error can remain.

The troposphere delay can be separated in a wet component due to water vapor and a dry component due to other atmospheric gases. While the dry delay can be modeled with high accuracy, the wet delay is a crucial component if accuracies in the decimeter or centimeter range are required, because of the high temporal and spatial variability of the water vapor content in the troposphere, although it contributes normally only with 5% to 15% of the total delay.

Since current global navigation satellite systems like GPS,

GLONASS and coming Galileo operate in L-band, attenuation by the atmosphere is negligible. This may change for next generation systems in the future, if additionally higher frequency bands are utilized, e.g. C-Band, which is already allocated for Galileo. However, also in L-band, occasionally, fast amplitude and phase scintillations can occur due to fast variations of the total electron content in the ionosphere or troposheric turbulences. Strong scintillations occur only rarely, but then they are critical and can even lead to complete loss of the navigation signals by the receiver.

Due to the extreme low signal power of the satellite navigation signals when arriving at the Earth, the signals can be easily attenuated and shadowed by buildings or vegetation, e.g. in urban or rural environments or in indoor applications. In these environments, additionally, multipath propagation by reflections of the signals by the ground, buildings and other obstacles before they arrive at the user antenna can significantly degrade the ranging and positioning accuracy. Multipath propagation is difficult to correct by models, because it depends strongly on the local user environment. Different techniques exist to mitigate the effect of multipath signals as far as possible either by advanced signal processing in receiver or by specially designed antennas, but multipath mitigation is still a hot topic of research.

REFERENCES

[1] B.W. Parkinson, "GPS Error Analysis," in *Global Positioning System, Theory and Applications*; Volume I, B.W. Parkinson B.W. and J. J. Spilker Jr., Ed. American Institute of Astronautics and Aeronautics, Washington DC, 1996.

[2] B. Hoffman-Wellenhof, H. Lichtenberger, and J. Collins., *Global Positioning System, Theory and Praxis*, Springer, Wien, New York; 4th edition, *1997.*

[3] A. Leick, *GPS Satellite Surveying*, John Wiley and Sons, New York, 1989.

[4] J. A. Klobuchar, " Ionospheric Effects on GPS," in *Global Positioning System, Theory and Application,* Volume I, B. W. Parkinson and J. J. Spilker Jr., Ed. American Institute of Astronautics and Aeronautics, Washington DC, 1996.

[5] J. A. Klobuchar, " Ionospheric Time-Delay Algorithm for Single-Frequency GPS Users," *IEEE Transactions on Aerospace and Electronic Systems*, Vol. AES-23, No.3, May 1987, pp. 325-331.

[6] ICD-GPS 200c, NAVSTAR GPS Space Segment/ Navigation User Interfaces, ARINC Research Corporation.

[7] G. D. Thayer, "An Improved Equation of Refractive Index of Air," *Radio Science*, Vol. 9, 1994, pp. 803-807.

[8] Mendes, V. B., Langley, R. B., "Tropospheric Zenith Delay Prediction Accuracy for High-Precision GPS Positioning and Navigation," *Journal of the Institute of Navigation*, Vol.46, No. 1, 1999, pp. 25-34.

[9] J. J. Spilker Jr.; "Tropospheric Effects on GPS," in *Global Positioning System, Theory and Application,* Volume I, B. W. Parkinson and J. J. Spilker Jr., Ed. American Institute of Astronautics and Aeronautics, Washington DC, 1996. pp. 517-546.

[10] H. S. Hopfield, "Two Quadratic Tropospheric Refractivity Profile for Correcting Satellite Data," *Journal of Geophysical Research*, Vol. 74, No.18, August 20, 1969, pp. 4487-4499.

[11] A. Hornbostel and M. M. Hoque, "Tropospheric Correction Models for Local Events," in Proc. *European Navigation Conf. GNSS* 2004, Rotterdam, 16-19 May 2004.

[12] *Galileo Reference Troposphere Description of Models*, Issue 1, Rev. 0, 25th March 2002, ESA-APPNG_SPEC/00165-AM.

[13] J. Saastamoinen, "Contributions to the Theory of Atmospheric refraction," *Bulletin Geodesique*, 1973, Vol.105, pp. 279-298, Vol.106, pp. 383-397, Vol.107, pp. 13-14.

[14] H. D. Black, "An Easily Implemented Algorithm for the Tropospheric Range Correction," *Journal of Geophysical Research*, Vol.83, No.B4, April 10, 1978, pp. 1825-1828.

[15] I. Ifadis, "The Atmospheric Delay of Radio Waves, Modeling the Elevation Dependence on a Global Scale," Technical Report no. 38L, School of Electrical and Computer Engineering, Chalmers University of Technology, Göteborg, Sweden 1986.

[16] C. C. Goad and L. Goodman, "A Modified Hopfield Tropospheric Refraction Correction Model," Presented Paper, *AGU Annual Fall Meeting*, San Francisco, 1974

[17] *Technical Characteristics of the NAVSTAR GPS*, NATO + NAVSTAR Technical Support Group, 1991.

[18] E.E Altshuler and P.M. Kalaghan, "Tropospheric range error corrections for the NAVSTAR system," AFCRL-TR-74-0198, April 1974.

[19] E.E. Altshuler, "Tropospheric Range-Error Correction for the Global Positioning System," *IEEE Trans. on Antennas and Propagation*, Vol. 46, No. 5, May 1998, pp. 643-649.

[20] *Minimum Operational Standard for global positioning/wide area augmentation system airborne equipment*, RTCA/DO-229A, June 8, 1998.

[21] *GALILEO Reference Troposphere Model for the User Receiver*, Issue 2, ESA, 10th July 2003.

[22] ESA Blind Model 2.3 issued on 28/01/2004 (MATLAB Code).

[23] A. Hornbostel and M.M. Hoque, "Analysis of Tropospheric Correction Models for Local Events within the GSTB Test Case APAF," in *Proc. of ION-GNSS 2004*, Institute of Navigation, Sept. 2004.

[24] A. Hornbostel, "Simulation of Tropospheric Effects for Satellite Navigation", in *Proc. European Telemetry Conference*, Garmisch, May 2000.

[25] http,//igscb.jpl.nasa.gov/components/prods.html

[26] *Propagation data and prediction methods required for the design of Earth-space telecommunication systems.*, ITU-R Rec. 618-4, 1994.

[27] G. H. Millman, "Tropospheric Effects on Space Communications," in *Proc. Conference on Tropospheric Radio Wave Propagation*, Part 1, AGARD Conference Proc. No. 70, pp. 4-1 - 4-29, 1970.

[28] *Attenuation in Vegetation*, ITU-R Rec. 833-2.

[29] W.C. Stone, *Electromagnetic Signal Attenuation in Construction Materials*, NIST Report 605, National Institute of Standards, Gaithersburg, Maryland, 1997.

[30] B. Eissfeller, A. Teuber, and P. Zucker, "Untersuchungen zum Satellitenempfang in Gebäuden," in *Allgemeine Vermessungsnachrichten* 4/2005, pp. 137–145. Herbert Wichmann Verlag, Heidelberg, 2005.

[31] H. Denks, "Übersicht über die geplanten Signale bei Galileo mit Schwerpunkt BOC-Signale," Technical Note, GalileoNAV-3100-1, Revision 1.2, DLR Institute of Communications and Navigation, 2003.

[32] O. Esbri-Rodriguez, A. Konovaltsev, and A. Hornbostel: "Modeling of the GNSS Directional Radio Channel in Urban Areas Based on Synthetic Environments," in *Proc. ION National Technical Meeting*, San Diego (USA), 26-28 January 2004.